Investigation of the Structural Stability of hUBF HMG Box 5 by Native-State Hydrogen Exchange†

Dandan Wang, Jiahai Zhang, Xianju Jin, Jihui Wu,* and Yunyu Shi*

Hefei National Laboratory for Physical Sciences at Microscale, School of Life Sciences, University of Science and Technology of China, Hefei, Anhui 230027, Peoples Republic of China

Received August 18, 2006; Revised Manuscript Received November 22, 2006

ABSTRACT: HMG box 5 of human upstream binding factor (hUBF) consists of three α-helices arranged in an L-shape with a hydrophobic core embraced by these helices and stabilized by extensive hydrophobic interactions between nonpolar residues around the core. The GdmCl-induced equilibrium unfolding transition of HMG box 5 of hUBF was monitored by both circular dichroism (CD) and fluorescence spectra. A cooperative two-state unfolding process was observed. The unfolding free energy, $\Delta G_U(D_2O)$, and the cooperativity of the unfolding reaction, m, are 4.6 ± 0.16 kcal·mol^{-1} and 1.62 ± 0.06 kcal·mol^{-1}·M^{-1}, respectively. Native-state hydrogen exchange (NHX) experiments under EX2 conditions were performed. NHX results clearly show that the hydrophobic core among the three helices is a slow-exchange core. The three helices would not contribute equally to the stability of the native protein. Helix 3 appears to contribute the least to the stability. The NHX data have also allowed the local, subglobal, and global unfolding structures of hUBF HMG box 5 to be dissected, and common global and subglobal unfolding units were successfully detected.

Understanding the mechanism of protein folding is central for unraveling the relationship between protein sequence, structure, stability, and function. Compared with other methods for studying protein folding, nuclear magnetic resonance (NMR) spectroscopy is unique in that it can monitor protein folding/unfolding reactions at atomic resolution (*1*, *2*). Hydrogen/deuterium exchange (HX) monitored by NMR spectroscopy is a powerful tool (*1*−*3*). The exchange rates of main chain NH protons with solvent deuterons depend on the protecting of hydrogen bonds existing in protein structure (*3*). Hydrogen bonds broken by a transient global unfolding reaction involved in most hydrogen bonds, by local fluctuation involved in individual bonds, or by subglobal unfolding reactions that break sets of neighboring hydrogen bonds can all be detected by HX measurement (*4*). It can provide direct information on the protein structure, structure change, interactions, dynamics, and folding, resolved to the level of individual amino acids (*4*, *5*).

Although HX measurement can be done over a wider range of denaturant concentration and temperature, the native-state HX method (NHX) has its own advantage (*3*). Under native conditions, though proteins exist predominantly in their native states to thermodynamic principles, low populations of partially folded intermediate state(s) and fully unfolded state could also exist (*3*, *6*−*9*). There is an equilibrium between unfolding and refolding. Most conventional biophysical probes, such as fluorescence or CD, are inadequate to detect this equilibrium under native conditions because they are all dominated by signals from the abundant native state (*9*−*11*). Conversely, NHX is a methodology wholly determined by those infinitesimally populated higher energy states, for the native state is the H/D exchange-incompetent state with regard to the majority of the slowly exchanging amide protons (*9*, *10*). By using amide proton exchange as the probe of protein folding, the NHX method not only is more sensitive toward the detection of partially folded conformations under native conditions but also can provide residue-specific structural information (*2*, *9*, *12*). Besides, this approach can provide useful insights about some other aspects, such as the ruggedness of the energy landscape, the various interactions stabilizing the native protein, and the correlation between the observed equilibrium intermediates with the kinetic intermediates (*12*).

The high mobility group (HMG) chromosomal proteins were discovered in mammalian cells more than 30 years ago (*13*, *14*). Subsequent studies have revealed that the functional motifs characteristic of the original, canonical HMG proteins are widespread among nuclear proteins from various organisms (*15*−*18*). The HMG proteins are subdivided into three superfamilies: HMGB, HMGN, and HMGA (*19*−*21*). The HMGB family is called the HMG box. Proteins in the HMG-box family usually consist of 70−80 amino acid residues and bind DNA in vitro with little or no sequence specificity (*22*, *23*). The global fold of the HMG box is well conserved and consists of three α-helices arranged in an L-shape with a hydrophobic core embraced by these helices and stabilized by extensive hydrophobic interactions between nonpolar residues around the core (*16*−*18*, *24*, *25*). The structures of

† This work was supported by the Chinese National Fundamental Research Project (Grants 2002CB713806 and 2004CB520500), the Chinese National Natural Science Foundation (Grants 30270293, 30121001, and 30570361), and the Pilot Project of the Knowledge Innovation Program of the Chinese Academy of Science (Grants KSCX1-SW-17 and KJCX2-SW-h14).

* To whom correspondence should be addressed. Tel: +86-551-3607464. Fax: +86-551-3601443. E-mail: yyshi@ustc.edu.cn, wujihui@ustc.edu.cn.

10.1021/bi061682r CCC: $37.00
Published on Web 01/10/2007

proteins in the HMG-box family are highly evolutionary conserved. All of these make the HMG box an interesting model for the studies of protein folding.

Human upstream binding factor (hUBF) belonging to the DNA binding protein family containing the DNA binding HMG box domain is important in the activation of rRNA gene transcription. It contains six tandemly arranged HMG-box domains (*16*, *23*). Within them, solution structures of hUBF HMG box 1 and hUBF HMG box 5 already reported by our laboratory show that they both adopt a twisted L-shape fold form, which is common to all of the other HMG domain structures (*16*, *23*). Apart from the structural studies, unfolding behaviors of hUBF HMG box 1 under different conditions were also observed. In that study, an intermediate-like state of hUBF HMG box 1 in the acid-induced unfolding process was successfully detected and then was further characterized (*26*, *27*). In order to get a more comprehensive understanding of the folding of the HMG box, we selected hUBF HMG box 5 as another model for the study and mainly focused our attention on observing the folding behavior of this protein under near-native conditions using NHX.

In this study, the NHX profile of hUBF HMG box 5 has been investigated as a function of GdmCl concentration, using denaturing conditions well below the unfolding transition region at pH 5.5. In contrast to the equilibrium unfolding events monitored by CD and fluorescence spectra, NHX data show that the hydrophobic core among the three helices is a slow exchange core. This hydrophobic core formed by three stacked aromatic rings of W14, W41, and W52 extends into other residues in the center region of helix 1 and helix 2. The three helices of hUBF HMG box 5 do not behave as a single cooperative unit. Helix 3 appears to contribute the least to the stability of the native protein. Residue W41 is not only a hydrophobic core contributing residue but also a residue playing key roles in stabilizing the loop between helix 2 and helix 3 by interacting with K49. The NHX data have also allowed the local, subglobal, and global structures of hUBF HMG box 5 to be dissected. Apart from the common global unfolding unit consisting of residues mostly in the central part of helix 1 and helix 2, a common subglobal unfolding unit with residues out of the hydrophobic core was also successfully detected.

MATERIALS AND METHODS

Buffers. D_2O and GdmCl used were ultrapure grade reagents from Calbiochem. All solutions were prepared with redistilled water and filtered through 0.22 μm pore size membranes before use. All other reagents used were of high quality analytical grade.

Protein Production. The hUBF HMG box 5 protein sample was purified completely according to the previous method described (*16*). Protein concentration was determined with the BCA protein assay kit, and the yield was ~23 mg/mL.

CD and Fluorescence Measurements. CD measurements were performed on a Jasco Model J-810 spectropolarimeter. In the far-UV region (195−250 nm), spectra were recorded with a 0.1 cm cell at a 0.15 mg/mL protein concentration, whereas in the near-UV region (250−300 nm), a 1 cm cell was used with a protein concentration of 1 mg/mL. Fluorescence emission spectra were recorded on a Thermo Spectronic Aminco-Bowman Series 2 luminescence spectrometer using a 1 cm cell. The measurements were performed using an excitation wavelength of 291 nm, and the spectra were recorded from 310 to 480 nm with a protein concentration of 18 μM. All of the spectra were measured two times at 22 °C, averaged, and corrected by subtraction of the solvent spectra obtained under identical conditions. F_U, K_U, and ΔG_U were acquired by using the equations (*28*):

$$F_U = (I_N - I)/(I_N - I_U) \quad (1)$$

$$K_U = (I_N - I)/(I - I_U) \quad (2)$$

$$\Delta G_U = -RT \ln K_U \quad (3)$$

where I is the observed spectrum intensity at a given GdmCl concentration, I_U is the spectrum intensity when the protein is completely unfolded, I_N is the spectrum intensity of the native protein, F_U is the fraction of unfolded protein at different GdmCl concentrations, K_U is the equilibrium constant for unfolding , and ΔG_U is the free energy change of unfolding.

Native-State HX Experiments. For preparation, different amounts of GdmCl, from 0.1 to 0.8 M in 20 mM sodium phosphate, pH 5.5, buffer were first lyophilized and then dissolved in D_2O. This was repeated three times. Meanwhile, each ^{15}N hUBF HMG box 5 protein sample (0.2 mM in 500 μL of 20 mM sodium phosphate, 100 mM sodium chloride, pH 5.5, buffer) was lyophilized. Before every H/D exchange experiment, GdmCl of a certain amount was first dissolved in D_2O so that the total volume of the solution was exactly 500 μL. Then a ^{15}N-labeled protein sample was dissolved in this denaturant−D_2O solution, immediately prior to data collection. All $^1H-^{15}N$ heteronuclear single-quantum coherence (HSQC) spectra were collected on a Bruker DMX500 spectrometer at 293 K. For samples at different GdmCl concentrations, $^1H-^{15}N$ HSQC spectra were first collected continuously for 12 h every 30 min and then collected back to back over a period of time until there were only several peaks left. The cross-peaks were assigned according to the existing assignments of hUBF HMG box 5. Cross-peak volumes instead of cross-peak intensities were determined to avoid artifacts arising upon addition of GdmCl. All of the NMR data processing was carried out using NMRPipe and NMRDraw software (*29*), and the data were analyzed with SPARKY. The decrease in the normalized peak volumes of each amide proton was measured as a function of time and fitted to single-exponential kinetics to obtain the exchange rate according to the equation:

$$I_t = I_0 + A \exp(-k_{ex}t) \quad (4)$$

where I_0 is the peak volume at time 0, I_t is the measured peak volume, A is the total change in the peak volume, and k_{ex} is the observed rate of HX.

The NHX Method Theory and Data Analysis. Amide protons involved in backbone hydrogen bonds are proposed to exchange with the solvent deuterium according to the scheme (*30*−*32*):

$$\text{NH(closed)} \underset{K_{op}}{\overset{K_{cl}}{\rightleftharpoons}} \text{NH(open)} \xrightarrow{K_{rc}} \text{exchange} \quad (5)$$

where k_{op} and k_{cl} are the opening and closing rates of the protecting structure and k_{rc} is the chemical exchange rate

constants of the amide proton as calculated from unfolded peptide models (*33*, *34*).

Under native conditions, there is an equilibrium preceding chemical exchange, with the open conformation being susceptible to exchange. This behavior is described by the equation:

$$k_{ex} = k_{op}k_{rc}/(k_{op} + k_{cl} + k_{rc}) \quad (6)$$

When $k_{cl} \gg k_{rc}$ (the EX2 limit), eq 6 reduces to eq 7. The measured exchange rate (k_{ex}) together with the known k_{rc} then provides K_{op} and hence ΔG_{HX}. In this way, the measurement of H/D exchange rates can provide site-specific information on the presence or absence of H-bond structure and its stability, dynamics, and other properties.

$$k_{ex} = (k_{op}/k_{cl})k_{rc} = K_{op}k_{rc} \quad (7)$$

$$\Delta G_{HX} = -RT \ln K_{op} = -RT \ln(k_{ex}/k_{rc}) \quad (8)$$

When at the EX1 limit where $k_{cl} \ll k_{rc}$, k_{ex} can be expressed as eq 9:

$$k_{ex} = k_{op} \quad (9)$$

where K_{op} is the equilibrium constant for transient opening of the protecting structure, ΔG_{HX} is the structural free energy difference between the closed and open states, R is the gas constant, and T is the absolute temperature at which the exchange was monitored.

A NHX strategy uses mildly destabilizing conditions to promote hydrogen exchange rate (*8*). The relationship between the free energy change associated with hydrogen exchange and denaturant concentration is often assumed to be linear (*35*) and is then given by the equation:

$$\Delta G_{HX}(\text{den}) = \Delta G_{HX}(0) - m[\text{GdmCl}] \quad (10)$$

where ΔG_{HX}(den) is the ΔG_{HX} for each amide proton at various concentrations of denaturant (GdmCl), $\Delta G_{HX}(0)$ is the stabilization free energy at zero denaturant concentration calculated from the acquired k_{ex}, and the slope, m, depends on the denaturant binding surface newly exposed in the unfolding reaction.

As mentioned above, three kinds of physical motions including global unfolding, subglobal unfolding, and local fluctuations can all lead from the native state to the exchange-competent states (*4*). As the measure of the degree of denaturant-accessible surface area, the m value can provide information on the nature of the physical motions (*36*, *37*). Local fluctuations are expected to exhibit near zero or smaller m values while global unfolding always shows the largest m values. If the unfolding process of the protein involves the accumulation of partially unfolded state(s), residues with m values in the intermediate range will be detected (*10*). In principle, amide protons participating in a common motion will exhibit m values in a common range. Because adding denaturant will selectively promote the partially unfolded and fully unfolded forms due to their larger m values (*5*, *8*, *9*), by examining the pattern of ΔG_{HX} versus GdmCl concentration of the amide protons, one can obtain the structural and energetic information of the different exchange-competent states. Some previous study suggested that under the EX2 experimental condition, the NHX data could be analyzed according to the three-component, local/subglobal/global equation (*38*):

$$\Delta G_{HX} = -RT \ln[\exp(-\Delta G_l/RT) + \exp(-\Delta G_{sg(w)}/RT - m_{sg}D) + \exp(-\Delta G_{g(w)}/RT - m_gD)] \quad (11)$$

Here, two-component exchange mechanisms were considered, and eq 12 was used for fitting of most of the HX curves:

$$\Delta G_{HX} = -RT \ln[\exp(-\Delta G_{HX}(0)/RT - m_1[\text{GdmCl}]) + \exp(-\Delta G_{HX}^*(0)/RT - m_2[\text{GdmCl}])] \quad (12)$$

where m_1 is the m value for the HX curve at no denaturant, $\Delta G_{HX}^*(0)$ is the ΔG_{HX} value at 0 M GdmCl acquired by linear extrapolation of the HX data at the linear part of the HX curves, and m_2 is the m value for the linear part of the HX curves. Goodness-of-fit tests for most of the observed amino amides indicate that eq 12 is sufficient to describe the data.

Protection factor (P) for the various amide protons in the protein was calculated from the equation:

$$P = k_{rc}/k_{ex} \quad (13)$$

RESULTS AND DISCUSSION

A Cooperative Two-State Unfolding Process Detected by CD and Fluorescence Spectra. The GdmCl-induced equilibrium unfolding transition of hUBF HMG box 5 was monitored by both CD and fluorescence techniques. CD spectra of hUBF HMG box 5 in its native and unfolded states measured in D_2O buffer are shown in Figure 1. When there is no GdmCl, the far-UV CD spectrum (Figure 1A) of this protein shows that there are two characteristic minima at about 208 and 222 nm, typical of proteins containing α-helical secondary structures. Its near-UV CD spectrum (Figure 1B) exhibits a profound negative band with minima at about 280 and 285 nm, which is an indication of aromatic side chains located in a nonpolar microenvironment that provide hydrophobic interactions stabilizing the tertiary structure of the protein. Thus, by following the ellipticities at 222 and 285 nm, it is easy to monitor the changes of the secondary and tertiary structures of hUBF HMG box 5 during the unfolding process induced by GdmCl. Figure 1 also shows CD signals of the protein in the presence of 6 M GdmCl. Under this situation, the shape of the CD spectrum changes dramatically and the ellipticity decreases to nearly zero, indicating the complete unfolding of this protein.

Denaturation of the native hUBF HMG box 5 in dependence on the concentration of GdmCl in D_2O buffer is shown in Figure 2A. The unfolding process fits a single transition curve which seems to be independent of the CD probes used to monitor it. Figure 2A exhibits the high cooperativity of the unfolding transitions. The secondary and tertiary structures of the protein denature approximately coincidental in the range of 1−4 M GdmCl with the midpoint denaturation concentration (C_m) at about 2.75 M. It therefore demonstrates that the GdmCl-induced equilibrium unfolding of hUBF HMG box 5 takes place via a two-state process without population of any stable equilibrium intermediates. The equilibrium unfolding transition of hUBF HMG box 5 was also monitored in H_2O solution, using far-UV CD at 222

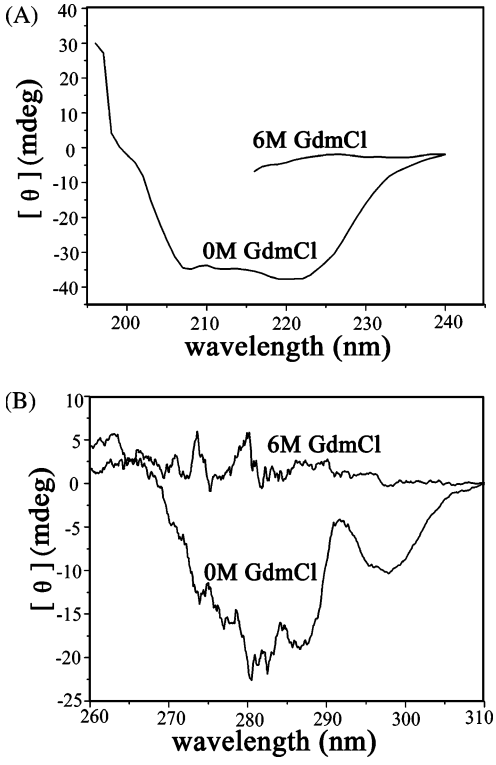

FIGURE 1: CD studies of hUBF HMG box 5 in D_2O. (A) Far-UV CD spectra of hUBF HMG box 5 under native conditions and in 6 M GdmCl. The protein concentration was 1.5 mg/mL in a 0.1 cm cell. (B) Near-UV CD spectra of hUBF HMG box 5 under native conditions and in 6 M GdmCl. The protein concentration was 1 mg/mL in a 1 cm cell. Spectra were recorded at 22 °C. Proteins were in 20 mM phosphate, pH 5.5, buffer supplemented with 100 mM NaCl.

nm as the structural probe. The unfolding transition curve obtained in H_2O by far-UV CD matches well with that obtained by near-CD in D_2O (Figure 2B), indicating that in both the H_2O and D_2O buffer hUBF HMG box 5 has the same structural stability. The values of the free energy of unfolding, ΔG_U (D_2O), and the measure of the cooperativity of the unfolding reaction, *m*, were determined to be 4.6 ± 0.16 kcal·mol^{-1} and 1.62 ± 0.06 kcal·mol^{-1}·M^{-1}, respectively.

The unfolding process of hUBF HMG box 5 monitored by the fluorescence technique in D_2O also exhibits a single transition curve with the C_m at about 2.75 M (data not shown), which is consistent with the CD results.

Hydrogen Exchange in hUBF HMG Box 5 Occurs through an EX2 Mechanism. There are two limits for the exchange. Exchange occurs by the EX2 (second-order reaction) limit, if refolding of the transient structural opening is fast compared with the intrinsic chemical exchange rate. Exchange by the EX1 (first-order reaction) limit is observed in special cases when the exchange is attributed to one-way unfolding above the unfolding transition or to transient global unfolding in destabilized proteins (*39*). In the present NHX study, the data analysis and the interpretation of the results both require the exchange behavior to correspond to the EX2 mechanism. Though EX2 is the dominating exchange regime for backbone amide protons in proteins and under exchange conditions used here, more likely to be the exchange mode acting, additional experiments must be done to further confirm this assumption. A simple way to tell EX2 from

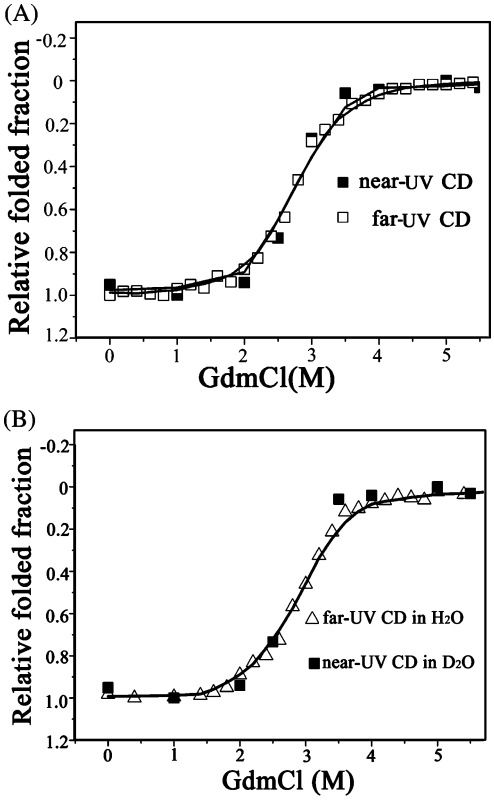

FIGURE 2: Two-state unfolding process detected by CD probes in D_2O buffer and the same structural stability of hUBF HMG box 5 measured in D_2O and H_2O. (A) GdmCl dependence of the unfolding process of hUBF HMG box 5 measured in D_2O. The secondary structure was followed by ellipticity at 222 nm (□) and the tertiary structure at 285 nm (■). (B) The unfolding transition curve of hUBF HMG box 5 obtained by near-UV CD in D_2O (■) matches well with that obtained by far-UV CD in H_2O (△). The relative folded fraction in Figure 2 was calculated by setting the least ellipticity value as 1 and the largest as 0. All spectra were recorded at 22 °C.

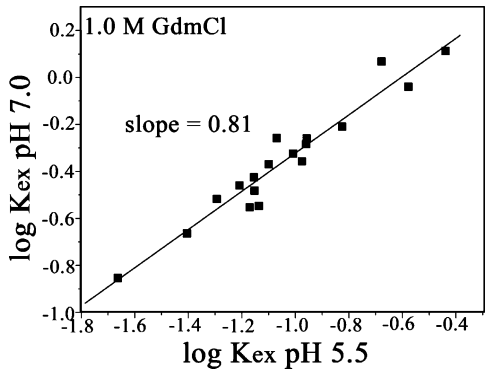

FIGURE 3: Plots of pH dependence of exchange at 1.0 M GdmCl. The value of log k_{ex} at pH 7.0 is plotted against the log k_{ex} at pH 5.5 for the same residue. Logarithms of amide proton exchange rates obtained at the two different pH conditions showed a linear correlation. The slope is 0.81 and the correlation coefficient is 0.97.

EX1 is to vary the pH at which exchange is carried out because the pH dependences of these two exchange modes are distinct. EX2 is the ideally pH-dependent exchange mode (*40, 41*). Such a test was carried out at 1.0 M GdmCl for hUBF HMG box 5 at two pH conditions (pH 5.5 and 7.0). Logarithms of amide proton exchange rates obtained at pH 5.5 and 7.0 showed a linear correlation (slope, 0.81) with a correlation coefficient of 0.97 (Figure 3), thus providing direct evidence that H/D exchange in hUBF HMG box 5

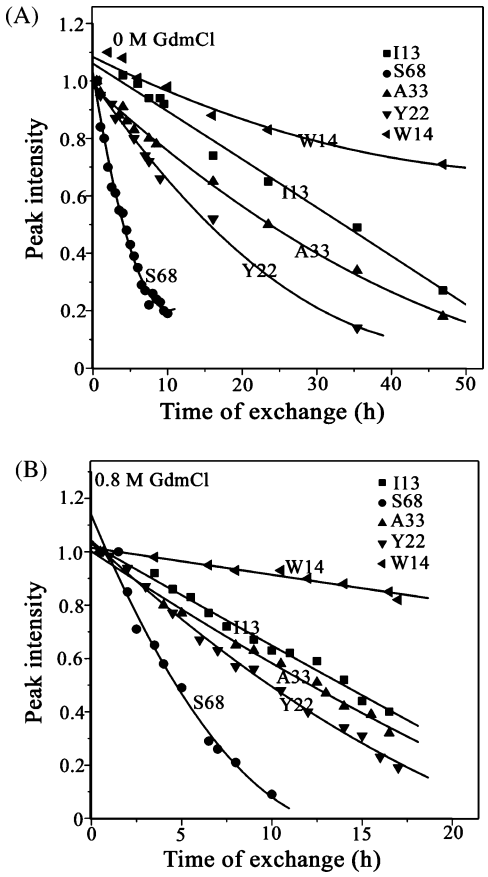

FIGURE 4: H/D exchange kinetics of the backbone amide proton of some representative residues at 0 and 0.8 M GdmCl. The solid lines through the data are fits to eq 4.

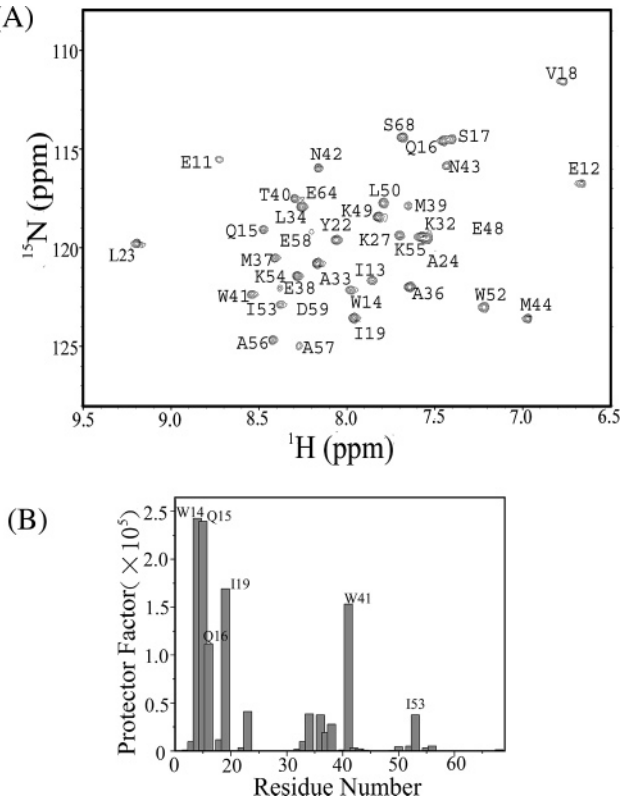

FIGURE 5: Representation of the ^{1}H−^{15}N HSQC spectrum of hUBF HMG box 5 and the protection factors for various amide protons at no denaturant. (A) The first two-dimensional ^{1}H−^{15}N HSQC NMR spectrum recorded in D_2O after initiation of exchange. All of the cross-peaks in the spectrum are well resolved and have been unambiguously assigned. (B) The protection factors estimated for all of the followed amide protons in hUBF HMG box 5 at 0 M GdmCl. Residues W14, Q15, Q16, I19, and W41 exhibit apparently higher protection factors.

under the given conditions (between pH 5.5 and pH 7.0) occurs predominately by the EX2 mechanism. Figure 4 is shown to illustrate the data quality of the H/D exchange experiments.

Hydrogen Exchange Kinetics and Different Local Stability. All of the cross-peaks in the first ^{1}H−^{15}N HSQC spectrum recorded after initiation of exchange are well-resolved and can be easily assigned, as was described before (*16* and Figure 5A). In all, exchange rates of 38 of the possible 84 amide protons could be measured at pH 5.5 at 293 K (Table 1). Forty-six main chain amide protons exchange out within the dead time of the measurement (10 min), most of which correspond to residues located in regions of irregular structure, either in the flexible regions of the protein (the two tails at the N- and C-termini) or in the loop region (Figure 6A and Table 1). Among the observed 38 residues, 15 exchange very fast, with rate constants (k_{ex}) greater than 1×10^{-2} min^{-1}. Twelve residues all belonging to the helical region exhibit moderately fast exchange rates (5×10^{-4} min^{-1} < k_{ex} < 1×10^{-2} min^{-1}) (Table 1). Nine residues, I13, W14, Q15, V18, I19, L34, M37, W41, and I53, are the slowest (k_{ex} < 5×10^{-4} min^{-1}) for exchange. These residues except I53 all belong to helix 1 and helix 2. From the structure, it was known that the conserved aromatic rings of W14, W41, and W52 stack into each other, forming a hydrophobic core to stabilize the structure of the protein. This core is extended into both arms and angle apexes. The packing of helix 1 into helix 2 also involves V18, I19, Y22, L34, and M37 (*16* and Figure 6B). This hydrophobic core is a slow-exchange core (Figure 6B and Table 1). Protection factors estimated for the various amide protons in native hUBF HMG box 5 are shown in Figure 5B. Five residues including W14, Q15, Q16, I19, and W41 show apparent higher protection factors than the other residues. In particular, residue W14 shows the largest protection factor (Figure 5B, $P = 2.43 \times 10^5$). Residue W41 shows a higher protection factor as expected. It is not only a hydrophobic core contributing residue but also a residue playing key roles in stabilizing the loop between helix 2 and helix 3 by interacting with K49 (*16* and Figure 6B). In helix 3, I53 rather than residue W52 shows a higher protection factor than the other residues in the same helix. It is easy to understand by taking into account that contact formed by this residue and R9/A10 is essential in determining the orientation of helix 1 and helix 3 (*16* and Figure 6B). The higher protection factor of I53 clearly illustrates the importance of maintaining the orientation of helix 1 and helix 3.

Helices Would Not Contribute Equally to the Structural Stability. Because the H/D exchange situation of amide protons depends on the protecting of protein structure and H-bonds, in HX experiments, residues exhibiting slower H/D exchange rates and higher protection factors are also those most likely taking part in forming H-bonds and other interactions in protein structures. In other words, from HX data, information about different contributions of various residues to the protein structural stability can be known. According to the NMR structure of hUBF HMG box 5, there

Table 1: H−D Exchange Patterns of Residues in hUBF HMG Box 5

rate constant (k_{ex}) range	residues
4×10^{-5} min^{-1} < k_{ex} < 5×10^{-4} min^{-1}	I13, W14, Q15, V18, I19, L34, M37, W41, I53
5×10^{-4} min^{-1} < k_{ex} < 1×10^{-2} min^{-1}	E12, Q16, Y22, L23, K32, A33, A36, E38, T40, K49, L50, W52, K55, A56, S68
$k_{ex} > 1 \times 10^{-2}$ min^{-1}	E11, S17, A24, K27, M39, N42, N43, M44, E48, K54, A57, A58, E59, E64
residues that exchange out in the dead time	G1−A10, G20, D21, R25, F26, N28−V31, K35, E45-K47, M51, Q60−Y63, R65−L67, E69−E84
the successfully followed 25 residues	E12−Q16, V18, I19, Y22, L23, K32−L34, A36, M37, E38, T40−M44, W52, I53, A56, S68

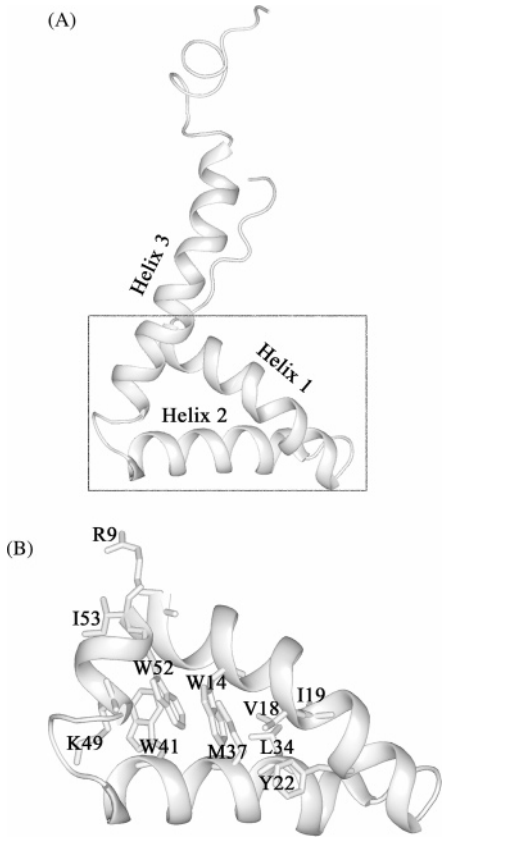

FIGURE 6: Representation of the solution NMR structure of hUBF HMG box 5 and some residues important in maintaining the fold of the protein. (A) PyMol cartoon drawing of the NMR structure of hUBF HMG box 5. The structural region in the dashed line frame is magnified in panel B. (B) Magnification of the special structural region in the dashed line frame indicated in panel A. Residues in the hydrophobic core and essential in maintaining the fold of the protein are shown in this graph.

are three helices located at sequence numbers 9−26, 30−42, and 48−70. They form an L-shape structure with helices 1 and 2 in one arm (the major wing) and helix 3 and N-terminal residues in the other arm (the minor wing) (*16*). There are two loops connecting helix 1, 2 and helix 2, 3. Evidence suggests that helix 3 contributes the least to the structural stability. First, among the successfully detected 38 residues, only 25 can be followed in the following experiments under various denaturing conditions. Though helix 3 is the longest helix in hUBF HMG box 5 (residues 48−70), among the 25 slow-exchange residues, only five belong to it. The high solvent susceptibility of most C-terminal residues in this helix is consistent with the NMR solution structure of this protein, as seen in Figure 6A. Second, for the five successfully followed residues in helix 3, the average protection factor value is distinctly lower than those for residues in the other two helices. Besides, only one of the nine slowest exchanging residues is located in helix 3. As to the other two helices, helix 1 and helix 2, the average protection factors are apparently higher. As was mentioned above, apart from the strong interactions between residues W14 and W41 in the hydrophobic core, the packing of these two helices also involves a number of other residues (Figure 6B). It seems likely that the packing regions of helix 1 and helix 2 constitute the stable core of the protein.

Global, Subglobal, and Local Unfolding Detected by NHX. In the H/D exchange experiment, according to eq 10, the relationship between unfolding free energy change and the denaturant concentration is linearly dependent. Slope, *m*, depends on the denaturant binding surface newly exposed to the unfolding reaction and is reflected in the exchange behavior of the slowly exchanging hydrogen (*42*). The change in accessible surface area (ΔASA) is related to the *m* value by the equation m (cal·mol^{-1}·M^{-1}) = 859 + 0.22 (ΔASA) (*43*). Hence, if there is no change in the accessible surface area upon addition of the denaturant, the minimum *m* value for the protein is expected to be 0.859 kcal·mol^{-1}·M^{-1}. On the basis of the minimum *m* value and the m value obtained previously by the CD analysis, H/D exchange profiles can be classified into three types: (1) The *m* value ≤ 0.9 in the whole range of denaturant. It is the local fluctuation type. As to this type, HX always occurs with little new solvent-accessible surface exposed. (2) The *m* value ≤ 0.9 at low GdmCl concentration and 0.9 < *m* < 1.6 at higher GdmCl concentration. This was categorized into the subglobal group. For residues in this group, the HX responsible opening reactions change from local fluctuation to subglobal unfolding. (3) The *m* value ≤ 0.9 at low GdmCl concentration and *m* ≥ 1.6 at higher GdmCl concentration. This is the global unfolding type. When denaturant concentration comes up to a certain point, HX in this group shows cooperative global unfolding behavior. For convenience, amide protons with HX curves belonging to the three types are called global, subglobal, and local fluctuation amide protons accordingly. This does not affect the conclusions drawn later. ΔG_{HX} values at various denaturants, *m* values, and the corresponding groups for all of the amide protons followed in the study are presented in Tables 2 and 3.

Figure 7A represents HX isotherms for eight residues, W14, Q15, Q16, L34, A36, E38, W41, and I53, amides of which belong to the global unfolding type. Among the eight residues, W14 and Q15 display a linear dependence of their ΔG_{HX} values even on very low GdmCl concentrations, implying that the amide protons of these two residues exchange merely through global unfolding processes. As to the other residues in the same group, the case is different. At low GdmCl concentrations, exchange of their amide protons appears to be dominated by local fluctuations with *m* values <0.9. When GdmCl concentration increases and reaches 0.7 M, global unfolding processes begin to dominate. L34, A36, and I53 have isotherm curves that extend smoothly toward the two linear lines. In contrast, isotherms of Q16 and W41 seem to be higher in energy compared with the

Table 2: ΔG_{HX} Values at Various Denaturant Concentrations for All of the Followed Residues in hUBF HMG Box 5

	G_{HX} values of exchange (kcal·mol^{-1})[a]								
residue	0 M GdmCl	0.2 M GdmCl	0.4 M GdmCl	0.6 M GdmCl	0.8 M GdmCl	1.0 M GdmCl	1.2 M GdmCl	1.4 M GdmCl	1.6 M GdmCl
E12	3.89	3.66	3.46	3.52	3.39	3.51	2.78		2.44
I13	5.31	5.10	5.19	4.99	4.85	4.75	4.47	4.43	4.18
W14	7.18		6.12	6.52	6.45	5.61	5.36	5.18	4.68
Q15	7.19	6.55	6.29	5.95	6.02	5.51	5.06	4.97	4.54
Q16	6.74	6.25	6.35	6.4	6.19	5.83	5.43	5.33	4.82
V18	5.43	5.18	5.20	5.54	4.86	4.69	4.85	4.59	3.96
I19	6.98		6.65		6.08	6.36	6.09		5.48
Y22	4.71	4.52	4.62	4.62	4.32	4.23	3.95	3.86	3.58
L23	6.16		5.84	5.93	5.85	5.57	5.32	5.33	4.91
K32	4.47	4.46	4.34	4.48	4.23	4.09	4.08	3.64	
A33	5.18	5.50	5.18	4.99	4.69	4.43	4.31	4.04	
L34	6.12	6.03	6.04	6.07	5.96	5.64	5.38	5.33	4.86
A36	6.11	5.94	6.10	6.12	6.01	5.58	5.26	5.15	4.79
M37	5.72	5.83	5.28	5.47	5.27	4.80	4.43	4.29	3.87
E38	5.93	5.64	5.69	5.78	5.64	5.40	5.19	5.06	4.75
T40	4.35	4.22	4.15	4.15	4.13	4.23	4.00	4.02	3.42
W41	6.92		6.86	6.99		6.31	5.99	5.87	5.41
N42	4.87		4.85	4.84	4.81	4.83	4.58	4.59	4.42
N43	4.58	4.43	4.53	4.49	4.52	4.64	4.44		4.37
M44	4.15	4.13	4.12	4.14	4.08	4.13	4.14	4.06	3.81
K49	3.73	3.77	3.73	3.71	3.70	3.58	3.38	3.37	3.15
W52	4.94	4.95	4.67	4.53	4.45	4.04	3.79	3.69	3.44
I53	6.11		5.70	5.88	5.83	5.33	5.06	4.97	4.62
A56	4.85	4.72	4.69	4.44	4.17	4.01			
S68	4.03	4.05	3.88	3.88	3.82	3.78	3.70	3.73	3.47

[a] For some residues, accurate G_{HX} values could not be determined because the rate of decay was too slow or too fast, or overlapping cross-peaks could not be deconvoluted under the experimental conditions.

Table 3: *m* Values, $\Delta G_{HX}(0)$ Values, and the Corresponding Amide Proton Groups for All of the Followed Residues of hUBF HMG Box 5

residue	*m* value (kcal·mol^{-1}·M^{-1})	group	$\Delta G_{HX}(0)$ (kcal·mol^{-1})	residue	*m* value (kcal·mol^{-1}·M^{-1})	group	$\Delta G_{HX}(0)$ (kcal·mol^{-1})
W14[a]	1.92 ± 0.14	global	7.18	I19	1.06 ± 0.13	subglobal	6.98
Q15[a]	1.65 ± 0.10	global	7.19	Y22	1.22 ± 0.04	subglobal	4.71
Q16	1.99 ± 0.10	global	6.74	L23	1.27 ± 0.07	subglobal	6.16
A33	1.98 ± 0.12	global	5.32	K32	1.27 ± 0.07	subglobal	4.32
L34	1.61 ± 0.04	global	6.12	T40	0.92 ± 0.09	subglobal	3.89
A36	1.89 ± 0.06	global	6.11	K49	0.93 ± 0.03	subglobal	3.73
M37	1.95 ± 0.07	global	5.72	W52[a]	1.0 ± 0.06	subglobal	4.94
E38	1.36 ± 0.06	global	5.94	A56	1.34 ± 0.04	subglobal	4.95
W41	2.04 ± 0.06	global	6.92	S68	1.11 ± 0.10	subglobal	4.03
I53	1.64 ± 0.08	global	6.11	N42	0.80 ± 0.04	local	4.66
E12	1.44 ± 0.03	subglobal	3.86	N43	0.17 ± 0.07	local	4.37
I13	1.09 ± 0.05	subglobal	5.31	M44	0.33 ± 0.05	local	3.87
V18	1.59 ± 0.13	subglobal	5.43				

[a] Residues are those *m* values which were acquired simply by linear fitting of the HX data.

two straight lines, indicating the existence of HX blocking residual structures in the unfolded state (*34*). Of the residues shown in Figure 7A, the *m* value of E38 is lower than that for global unfolding. Because at higher denaturants this residue also joins the global unfolding, the amide proton of it is considered to exchange from the fully unfolded state as well. It is interesting that residues in this group with the exception of I53 all belong to the central segment of helix 1 or helix 2. At low denaturant concentration (<0.7 M), these residues except W14 and Q15 all exhibit local fluctuation exchange behavior. When the denaturant concentration reaches 0.7 M that is much lower than the midpoint denaturation concentration C_m, 2.75 M, in the equilibrium unfolding curve, the state of amide protons in this group changes cooperatively from the nonexchangeable protected state to the unprotected state. Significant exposure of the buried surface happened.

Among all of the subglobal unfolding amide protons shown in Figure 7B,C, only amide W52 has the HX isotherm linearly dependent even on low GdmCl concentrations. HX curves higher in energy than that for W52 are shown in Figure 7B, and those lower are in Figure 7C. All residues, coincidentally all in helix 1, in Figure 7B show exchange dominated by local fluctuations at low GdmCl concentrations, whereas at higher denaturant concentrations, exchange appears to be dominated by subglobal unfolding. HX isotherm curves in this figure show consistent dispersion and do not merge to a single subglobal curve. Usually when the denaturant concentration increases, the dispersion would narrow down and finally merge together to define one or more partially folded structural units (*6*, *7*, *9*, *12*), though considerable dispersion in ΔG_{HX} curves has also been seen in a number of other proteins. Two reasons may account for the results observed here. First, taking into account the *m*

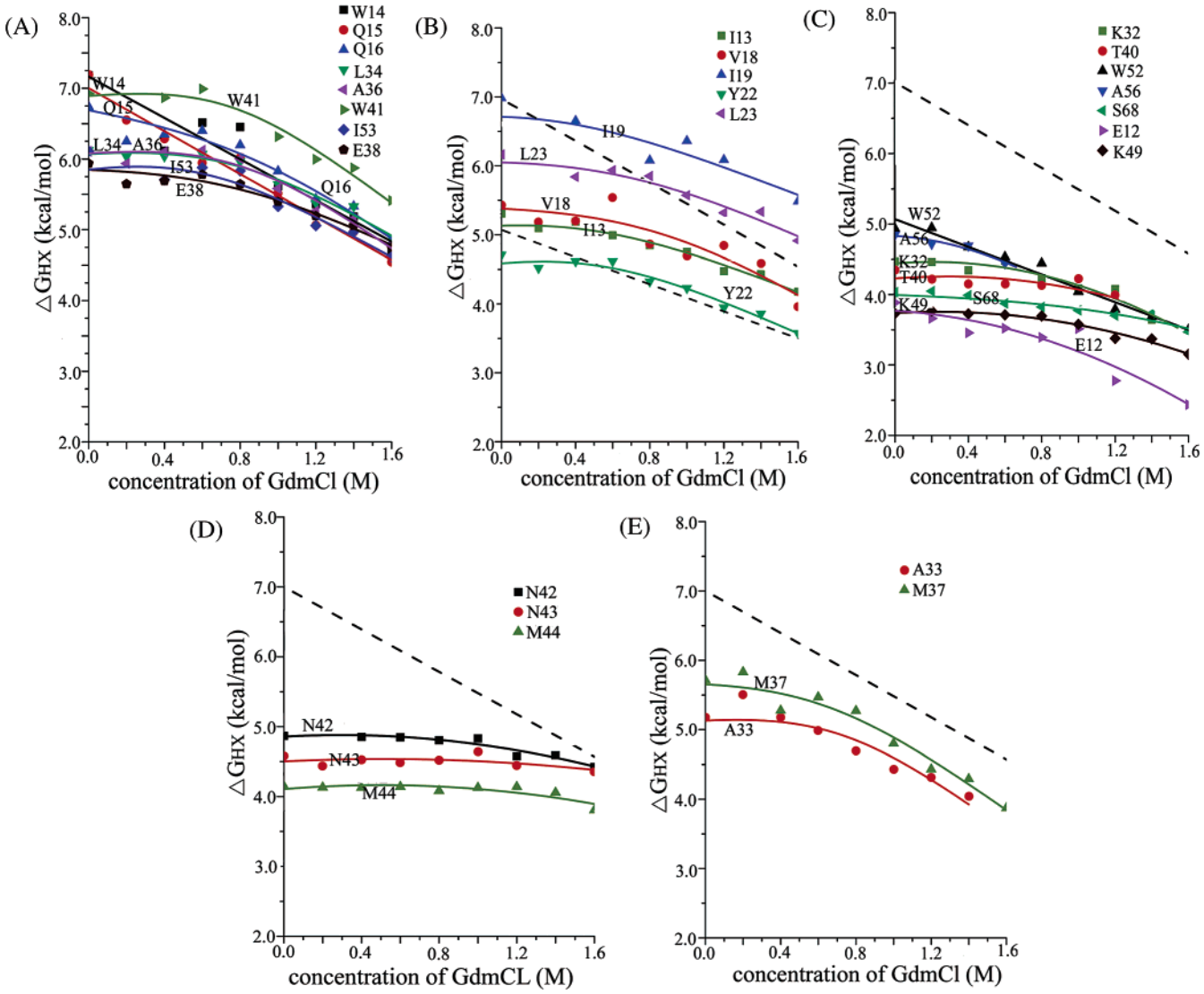

FIGURE 7: Native-state hydrogen exchange results of hUBF HMG box 5. (A) The results of global unfolding amide protons. (B) Subglobal unfolding amide protons with HX curves higher in energy than that for W52. The upper dotted line represents the isotherm of amide Q15 and the lower represents that of amide W52. (C) HX isotherm for amide W52 and isotherms lower in energy than that for W52. The dotted line represents the HX isotherm of amide Q15. (D) Local fluctuations of amide protons. The dotted line represents the HX isotherm of amide Q15. (E) Isotherms for residues A33 and M37. The dotted line represents the HX isotherm of amide Q15.

values of these amide protons, it is reasonable to assume that even at those higher GdmCl concentrations local fluctuations still contribute much, and it is known that exchange of amide protons occurring through local fluctuations always has very different rates and ΔG_{HX} values (*7*). It is also possible that several structure-opening equilibria, representing multiple protein conformations closely spaced in energy, are operative in the exchange of protein amide protons as in the case of T4 and reduced horse cytochrome *c* (*44*, *45*). In this figure, HX curves of I19 and L23 are higher in energy than the upper dotted line (HX profile of residue Q15), indicating that some residual structures of these two residues still remain in those unfolded protein conformations.

All residues, K32, T40, K49, W52, A56, and E68, except E12 presented in Figure 7C belong to helix 2 and helix 3. In this figure, W52 shows a linear dependence of its ΔG_{HX} values on GdmCl concentration with an *m* value of 1.0 kcal·mol^{-1}·M^{-1}. In NHX, partially unfolded forms (PUFs) are usually identified according to observing HX isotherms linearly dependent on denaturant concentrations with a lower *m* value than the value for global unfolding. Thus, the isotherm of W52 can be used to define a PUF of hUBF HMG box 5. The unfolding free energy of this PUF is 4.94 kcal·mol^{-1}, equal to the $\Delta G_{HX}(0)$ value of amide W52. At higher denaturant concentration, sets of amide protons belonging to residues which include K32, T40, A56, and E68 all merge into the same linear isotherm. From the HX curves shown in Figure 7C, one conclusion can be reasonably drawn that these residues form a cooperative unfolding unit. It seems that when W52 is unfolded, residues including K32, T40, A56, and E68 are also unfolded. These residues are out of the hydrophobic core. ΔG_{HX} values for them are lower than the values for residues in the hydrophobic core. The slope of the HX curves for these amide protons matches the subglobal *m* value. K49 is a residue at the N termini of helix 3, so its amide proton displays exchange behavior mostly like local fluctuations with the *m* value of only 0.92. E12 has the lowest ΔG_{HX} value compared with all of the other residues followed in the study. This residue is located in the

so-called Y position, which is very important in mediating the binding of the HMG box and DNA (*16*). From this figure and Figure 7A, HX behavior differences between I53 and the other residues in helix III can be easily seen. HX of amide I53 happens with a $\Delta G_{HX}(0)$ value of 6.11 kcal·mol^{-1} (Table 3), which is higher than the free energy of the PUF defined by residue W52. And unlike other subglobal amide protons in helix III, amide I53 belongs to the global unfolding type according to its *m* value of 1.64 ± 0.08 kcal·mol^{-1}·M^{-1} (Table 3). These differences indicate that, in the partially unfolded form, helix III is not fully unfolded. Maybe in the special unfolded form, contacts crucial for the orientation between helix III and helix I formed by I53 and some other residues still remain.

Figure 7D shows HX isotherms for only three residues, N42, N43, and M44, H/D exchange of which seems to be always dominated by local fluctuations. N42 is the residue at the end of helix 2 and N43 and M44 are two loop region residues. Compared with other residues in the loop region, N43 and M44 are in a partially helical conformation (*16*). That may be why HX of the amide protons of the two residues can be detected in the study. H/D exchange behavior of amide M37 and A33 cannot be categorized into each of the three groups (Figure 7E). Though the *m* values associated with M37 and A33 belong to the global unfolding group, the HX isotherms for them are lower in energy than that for global unfolding. It may indicate that some particular protein conformations exist. Though in these particular states the degree of denaturant-accessible surface area exposed is nearly equal to that exposed by the globally unfolded state, HX of some amide protons becomes somewhat easier.

From the NHX results discussed above, it is apparent that amide protons in the central part rather than in a continuous region of secondary structure of the hUBF HMG box 5 display uniform exchange behavior. For example, in helix 1, all of the global unfolding amide protons belong to residues in the central region, while residues at the edge of this helix show subglobal exchange behavior.

Discrepancy between ΔG_{HX} *and* ΔG_U. The ΔG_U value obtained from CD measured in D_2O is 4.6 ± 0.16 kcal·mol^{-1}. This value is lower than most of the ΔG_{HX}*(0) values indicated by residues in hUBF HMG box 5. Several factors could account for the observed difference (*35*, *42*, *46*). First, the ΔG_U value measured by GdmCl denaturation experiments could be affected by the presence of undetected intermediates and the non-native solvent conditions presented by the high concentrations of GdmCl. Second, there are four *trans*-prolines in hUBF HMG box 5. The slow *cis*−*trans* proline isomerization of the prolyl peptide bond in the unfolded state(s) will lead to a discrepancy between ΔG_{HX} and ΔG_U because an equilibrium between *cis* and *trans* forms is reached in the denaturant-induced unfolding measurements but not in the H/D exchange experiment (*35*, *42*). For each proline, the correction is 0.5 kcal·mol^{-1}, assuming a *cis*/*trans* ratio of 0.25 in the equilibrium unfolded state. So, the total correction is 2 kcal·mol^{-1}, which can significantly account for the observed discrepancy. Third, the extrapolation of GdmCl denaturation data from the transition region to 0 M denaturant may not be linear, but in fact curves upward. Apart from the three reasons, like the four residues (Q16, I19, L23, and W41), some residues may still have residual structures in the unfolded protein. These residual structures can protect the amide protons from exchange, thus enhancing the ΔG_{HX} values. The difference between ΔG_{HX} and ΔG_U observed in hUBF HMG box 5 could arise due to one or more of the reasons discussed above.

Implications for the Protein Folding. The H/D exchange method has been widely used to study the folding problem for a number of proteins (*6*, *7*, *47*, *48*). Some of these studies suggest a common stepwise stabilization strategy using intrinsic cooperative secondary structures as building blocks, as in the case of cytochrome *c*, RNase H, and Rd-apocyt b_{562} (*6*, *7*, *47*). For other studies, "the slow exchange core is the folding core" model was proposed (*48*). This model does not suggest the order of folding for secondary structural elements outside the slow-exchange core; instead, it implies that the most favored conformation of a protein sampled early in folding tends to involve native-like interactions between clusters of residues that eventually fold into the slow-exchange core (*48*). For hUBF HMG box 5, the hydrophobic core is the slow-exchange core. All of the residues except W52 in the hydrophobic core belong to the packing region of helix 1 and helix 2. That region constitutes the most stable part of the native protein. On the basis of the NHX results, the possible folding process of hUBF HMG box 5 can be assumed as follows. After the packing region forms the folding core, it is most likely that contacts crucial for the orientation between helix 1 and helix 3 begin to form, for the orientation of the highly correlated residue I53 is the most protected one in all of the helix 3 residues. Finally, additional contacts between helix 3 and the other two helices develop and further stabilize the native protein. In spite of the resemblance between the protein folding core and the slow-exchanging core observed for several proteins, Fersht and co-workers, on the basis of their studies on barnase and chymotrypsin inhibitor 2, showed that there is no obvious relationship between hydrogen exchange at equilibrium and their folding pathways (*49*). To more clearly understand the folding processes of hUBF HMG box 5, further HX pulse labeling experiments have to be conducted.

ACKNOWLEDGMENT

We thank all of the members of our laboratory, past and present, who have contributed to this work. We also thank Dr. F. Delaglio and Prof. A. Bax for providing the software NMRPipe and Prof. T. D. Goddard and Prof. D. G. Kneller for providing SPARKY.

REFERENCES

1. Dyson, H. J., and Wright, P. E. (1996) Insights into protein folding from NMR, *Annu. Rev. Phys. Chem. 47*, 369−395.
2. Juneja, J., and Udgaonkar, J. B. (2003) NMR studies of protein folding, *Curr. Sci. 84*, 157−172.
3. Krishna, M. M. G., Hoang, L., Lin, Y., and Englander, S. W. (2004) Hydrogen exchange methods to study protein folding, *Methods 34*, 51−64.
4. Englander, S. W., Mayne, L., Bai, Y., and Sosnick, T. R. (1997) Hydrogen exchange: The modern legacy of Linderstrøm-Lang, *Protein Sci. 6*, 1101−1109.
5. Maity, H., Lim, W. K., Rumbley, J. N., and Englander, S. W. (2003) Protein hydrogen exchange mechanism: Local fluctuations, *Protein Sci. 12*, 153−160.
6. Chu, R., Pei, W., Takei, J., and Bai, Y. (2002) Relationship between the native-state hydrogen exchange and folding pathways of a four-helix bundle protein, *Biochemistry 41*, 7998−8003.

7. Maity, H., Maity, M., Krishna, M. M. G., Mayne, L., and Englander, S. W. (2005) Protein folding: The stepwise assembly of foldon units, *Proc. Natl. Acad. Sci. U.S.A. 102*, 4741−4746.
8. Hoang, L., Bedard, S., Krishna, M. M. G., Lin, Y., and Englander, S. W. (2002) Cytochrome *c* folding pathway: Kinetic native-state hydrogen exchange, *Proc. Natl. Acad. Sci. U.S.A. 99*, 12173−12178.
9. Rumbley, J., Hoang, L., Mayne, L., and Englander, S. W. (2001) An amino acid code for protein folding, *Proc. Natl. Acad. Sci. U.S.A. 98*, 105−112.
10. Chi, Y., Kumar, T., Chiu, I., and Yu, C. (2002) Identification of rare partially unfolded states in equilibrium with the native conformation in an all β-barrel protein, *J. Biol. Chem. 277*, 34941−34948.
11. Spudich, G., Lorenz, S., and Marqusee, S. (2002) Propagation of a single destabilizing mutation throughout the *Escherichia coli* ribonuclease HI native state, *Protein Sci. 11*, 522−528.
12. Bhutani, N., and Udgaonkar, J. B. (2003) Folding subdomains of thioredoxin characterized by native-state hydrogen exchange, *Protein Sci. 12*, 1719−1731.
13. Erlandsson, H., and Andersson, H. U. (2004) The nuclear protein HMGB1 as a proinflammatory mediator, *Eur. J. Immunol. 34*, 1503−1512.
14. Teng, C. T., and Teng, C. S. (1981) Changes in quantities of high-mobility-group protein 1 in oviduct cellular fractions after oestrogen stimulation, *Biochem. J. 198*, 85−90.
15. Grasser, K. D. (1995) Plant chromosomal high mobility group (HMG) proteins, *Plant J. 7*, 185−192.
16. Yang, W., Xu, Y., Wu, J., Zeng, W., and Shi, Y. (2003) Solution structure and DNA binding property of the fifth HMG box domain in comparison with the first HMG box domain in human upstream binding factor, *Biochemistry 42*, 1930−1938.
17. Jones, D. N., Searles, M. A., Shaw, G. L., Churchill, M. E., Ner, S. S., Keeler, J., Travers, A., and Neuhaus, A. D. (1994) The solution structure and dynamics of the DNA-binding domain of HMG-D from *Drosophila melanogaster*, *Structure 2*, 609−627.
18. Masse, J. E., Wong, B., Yen, Y. M., Allain, F. H, Johnson, R. C., and Feignon, J. (2002) The *S. cerevisiae* architectural HMGB protein NHP6A complexed with DNA: DNA and protein conformational changes upon binding, *J. Mol. Biol. 323*, 263−284.
19. De, D. N. (2002) Protein constitution of the chromosome axis, *Chromosoma 111*, 69−79.
20. Catez, F., Yang, H., Tracey, K. J., Reeves, R., Misteli, T., and Bustin, M. (2004) Network of dynamic interactions between histone H1 and high-mobility-group proteins in chromatin, *Mol. Cell. Biol. 24*, 4321−4328.
21. Beitzel, B., and Bushman, F. (2003) Construction and analysis of cells lacking the HMGA gene family, *Nucleic Acids Res. 31*, 5025−5032.
22. Jantzen, H. M., Admon, A., Bell, S. P., and Tjian, R. (1990) Nucleolar transcription factor hUBF contains a DNA-binding motif with homology to HMG proteins, *Nature 344*, 830−836.
23. Xu, Y., Yang, W., Wu, J., and Shi, Y. (2002) Solution structure of the first HMG box domain in human upstream binding factor, *Biochemistry 41*, 5415−5420.
24. Weir, H. M., Kraulis, P. J., Hill, C. S., Raine, A. R., Laue, E. D., and Thomas, J. O. (1993) Structure of the HMG box motif in the B-domain of HMG1, *EMBO J. 12*, 1311−1319.
25. Read, C. M., Cary, P. D., Crane-Robinson, C., Driscoll, P. C., Carillo, M. O. M., and Norman, D. G. (1995) The structure of the HMG box and its interactions with DNA, *Nucleic Acids Mol. Biol. 9*, 222−250.
26. Zhang, X., Zhang, J., Li, X., Xu, J., Huang, H., Chen, Q., Wu, J., and Shi, Y. (2004) Compact molten globule-like state of hUBF Box 1 at extremely low pH, *Biochim. Biophys. Acta 1748*, 66−73.
27. Zhang, X., Xu, Y., Zhang, J., Wu, J., and Shi, Y. (2005) Structural and dynamic characterization of the acid-unfolded state of hUBF HMG box 1 provides clues for the early events in protein folding, *Biochemistry 44*, 8117−8125.
28. Viguera, A. R., Martinez, J. C., Filimonov, V. V., Mateo, P. L., and Serrano, L. (1994) Thermodynamic and kinetic analysis of the SH3 domain of spectrin shows a two-state folding transition, *Biochemistry 33*, 2142−2150.
29. Delaglio, F., Grzesiek, S., Vuister, G. W., Zhu, G., Pfeifer, J., and Bax, A. (1995) NMRPipe: a multidimensional spectral processing system based on UNIX pipes, *J. Biomol. NMR 6*, 277−293.
30. Linderstrøm-Lang, K. (1955) Deuterium exchange between peptides and water, *Chem. Soc., Spec. Publ. 2*, 1−20.
31. Hvidt, A., and Nielsen, S. O. (1966) Hydrogen exchange in proteins, *Adv. Protein Chem. 21*, 287−386.
32. Englander, S. W., and Kallenbach, N. R. (1983) Hydrogen exchange and structural dynamics of proteins and nucleic acids, *Q. Rev. Biophys. 16*, 521−655.
33. Bai, Y., Milne, J. S., Mayne, L., and Englander, S. W. (1993) Primary structure effects on peptide group hydrogen exchange, *Proteins 17*, 75−86.
34. Bai, Y., Milne, J. S., Mayne, L., and Englander, S. W. (1994) Protein stability parameters measured by hydrogen exchange, *Proteins 20*, 4−14.
35. Schellaman, J. A. (1987) The thermodynamic stability of proteins, *Annu. Rev. Biophys. Biophys. Chem. 16*, 115−137.
36. Bai, Y., Karimi, A., Dyson, H. J., and Wright, P. E. (1997) Absence of a stable intermediate on the folding pathway of protein A, *Protein Sci. 6*, 1449−1457.
37. Yi, Q., and Baker, D. (1996) Direct evidence for a two-state protein unfolding transition from hydrogen-deuterium exchange, mass spectrometry, and NMR, *Protein Sci. 5*, 1060−1066.
38. Parker, M. J., and Marqusee, S. (2001) A kinetic folding intermediate probed by native state hydrogen exchange, *J. Mol. Biol. 305*, 593−602.
39. Englander, S. W., Sosnick, T. R., Englander, J. J., and Mayne, L. (1996) Mechanisms and uses of hydrogen exchange, *Curr. Opin. Struct. Biol. 6*, 18−23.
40. Meisner, W. K., and Sosnick, T. R. (2004) Barrier-limited, microsecond folding of a stable protein measured with hydrogen exchange: Implications for downhill folding, *Proc. Natl. Acad. Sci. U.S.A. 101*, 15639−15644.
41. Viguera, A., and Serrano, L. (2003) Hydrogen-exchange stability analysis of Bergerac-Src homology 3 variants allows the characterization of a folding intermediate in equilibrium, *Proc. Natl. Acad. Sci. U.S.A. 100*, 5730−5735.
42. Bai, Y., and Englander, S. W. (1996) Future directions in folding: the multi-state nature of protein structure, *Proteins 24*, 145−151.
43. Myers, J. K., Pace, C. N., and Scholtz, J. M. (1995) Denaturant m values and heat capacity changes: relation to change in accessible surface areas of protein folding, *Protein Sci. 4*, 2138−2148.
44. Bhuyan, A. K., and Udgaonkar, J. B. (1998) Stopped-flow NMR measurement of hydrogen exchange rates in reduced horse cytochrome *c* under strongly destabilizing conditions, *Proteins 32*, 241−247.
45. Llinas, M., Gillespie, B., Dahlquist, F. W., and Marqusee, S. (1999) The energetics of T4 lysozyme reveal a hierarchy of conformations, *Nature 6*, 1072−1078.
46. Williams, N. K., Liepinsh, E., Watt, S. J., Prosselkov, P., Matthews, J. M., Attard, P., Beck, J. L., Dixon, N. E., and Otting, G. (2005) Stabilization of native protein fold by intein-mediated covalent cyclization, *J. Mol. Biol. 346*, 1095−1108.
47. Chamberlain, A. K., Handel, T. M., and Marqusee, S. (1996) Detection of rare partially folded molecules in equilibrium with the native conformation of RNaseH, *Nat. Struct. Biol. 3*, 782−787.
48. Li, R., and Woodward, C. (1999) The hydrogen exchange core and protein folding, *Protein Sci. 8*, 1571−1591.
49. Clarke, J., Itzhaki, L. S., and Fersht, A. R. (1997) Hydrogen exchange at equilibrium: a short cut for equilibrium: a short cut for analyzing protein-folding pathways?, *Biochem. Sci. 22*, 284−287.

BI061682R